Centrifuge Study of Downdrag on Axially Loaded Piles in Liquefiable Soils

Centrifugeuse étude d'abaissement sur des pieux chargés axialement dans les sols liquéfiables

Sumeet Sinha, Katerina Ziotopoulou & Bruce Kutter
Civil and Environmental Engineering, University of California Davis, USA, skssinha@ucdavis.edu

ABSTRACT: Piles are designed to transfer superstructure loads using positive skin friction and tip resistance while undergoing acceptable settlements. However, when liquefaction-induced soil settlement occurs, it can drag the pile downward and result in negative skin friction and drag load. In such cases, estimating the drag load and pile settlement becomes important for pile design. A series of centrifuge model tests were performed to study liquefaction-induced downdrag on piles. The tests included four heavily instrumented piles installed in two different soil layered profiles with their tip embedment zero, three and five times their diameter in the dense sand. Loads on the piles were varied to study their effect on drag load and pile settlement. Results are presented describing the mechanism behind the development of liquefaction-induced downdrag, the magnitude of drag load, and pile settlement. Finally, recommendations are made for the design of piles in liquefiable soils.

RÉSUMÉ : Les pieux sont conçus pour transférer les charges de la superstructure en utilisant un frottement de peau positif et une résistance de pointe tout en subissant des tassements acceptables. Cependant, lorsque le tassement du sol induit par la liquéfaction se produit, il peut entraîner le pieu vers le bas et entraîner un frottement négatif de la peau et une charge de traînée. Dans de tels cas, l'estimation de la charge de traînée et du tassement des pieux devient importante pour la conception des pieux. Une série d'essais sur modèle de centrifugation a été réalisée pour étudier la traînée descendante induite par la liquéfaction sur les pieux. Les tests comprenaient quatre pieux fortement instrumentés installés dans deux profils de couches de sol différents avec leur ancrage de pointe nul, trois et cinq fois leur diamètre dans le sable dense. Les charges sur les pieux ont été variées pour étudier leur effet sur la charge de traînée et le tassement des pieux. Les résultats sont présentés décrivant le mécanisme derrière le développement de la traînée descendante induite par la liquéfaction, l'ampleur de la charge de traînée et le tassement du pieu. Enfin, des recommandations sont faites pour la conception des pieux dans les sols liquéfiables.

KEYWORDS: downdrag, drag load, piles, liquefaction, centrifuge

1 INTRODUCTION

Piles are designed to transfer loads to greater soil depths and more capable strata through skin friction and tip resistance while undergoing acceptable settlement relative to the tolerances of the supported structure. Pile settlement relative to the downward moving soil is only relevant with respect to the magnitude of unit negative shaft resistance. Under normal conditions, the pile resists the superstructure load by mobilizing positive skin friction around its shaft and tip resistance at its toe, resulting in an overall decrease of axial load with depth. However, when earthquake-induced liquefaction occurs, reconsolidation in the liquefied layers results in soil settlement around the pile (Figure 1). The phenomenon of drag on a pile from the settlement of soil surrounding it is known as downdrag. If the settlement of soil around the shaft exceeds the movement of the pile, negative skin friction is generated. The developed negative skin friction adds an internal load on the pile known as drag load (Figure 1(b)). As a result, the overall load on the pile increases with depth until the pile experiences positive skin friction, after which it starts to decrease. The depth at which the soil and the pile settle the same (i.e., their relative movement is zero) is known as the neutral plane (see Figure 1(b)). Above the neutral plane, the relative movement of the soil is greater than the pile resulting in the development of negative skin friction and drag loads. Below the neutral plane, the relative movement of the pile is greater than the surrounding soil resulting in the development of positive skin friction that resists the loads on the pile. Overall, the load on the pile increases while the length of the pile resisting the load decreases. As a result, more load is transferred to the tip, and the pile settles until a force equilibrium is achieved. Estimating the drag load and the pile settlement is thus important for designing and evaluating the performance of piles in liquefiable soils.

Estimating the drag load for pile design requires estimating the neutral plane and the mobilized negative skin friction in the liquefiable and non-liquefiable layers above it. Pile settlement can be calculated from the tip movement required to mobilize tip resistance to balance the overall load at the neutral plane. The current state of practice AASHTO (2020) assumes negative skin friction equal to the residual shear strength of soil in the liquefiable zone and ultimate interface strength in the non-liquefiable layers. Fellenius and Siegel (2008) recommend using the unified pile design method (Fellenius 1984; Fellenius 2004) with zero negative skin friction in the liquefiable layers to estimate the drag load and pile settlement. Boulanger and Brandenberg (2004) proposed a modified neutral plane method to estimate the development of negative skin friction and pile settlement during reconsolidation. The method assumed full mobilization of interface friction linearly factored with the excess pore pressure in soil. Through blast-induced liquefaction studies, Rollins and Strand (2006) recommended the negative skin friction in the liquefiable layer as approximately 50% of the positive skin friction before liquefaction. However, in blast-induced liquefaction test conducted on sites with earthquake drains, Rollins and Strand (2007) observed the negative skin

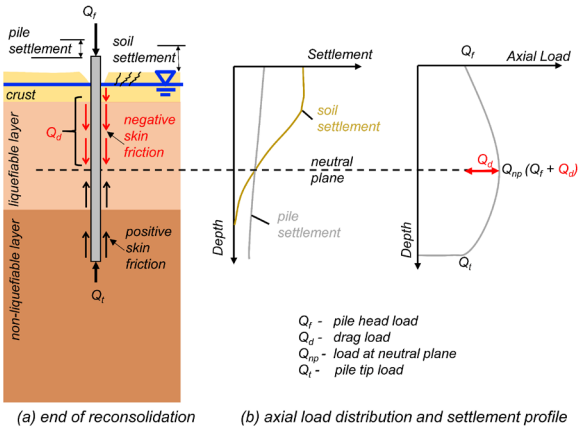

Figure 1. Illustration of liquefaction-induced downdrag on piles.

friction equal to 100% of the positive skin friction before liquefaction. Caltrans (2020) and Federal Highway Administration (FHWA) (Hannigan et al. 2016) recommend the use of the neutral plane method with soil behavior models (t-z and q-z models) calibrated from the field tests to determine the drag load and pile settlement. While the studies mentioned above have improved our understanding of liquefaction-induced downdrag, there is still some confusion in estimating the negative skin friction in the liquefiable layer and pile settlement. More testing is required to understand the development of drag load and pile settlement in liquefiable layers.

In the present study, centrifuge model tests were performed to study liquefaction-induced downdrag on piles. Four heavily instrumented piles with their tip embedded zero to five times their diameter in dense sand were tested in two soil profiles with varying loads resulting in static safety factors ranging from 2.5 to 12. Results illuminate the mechanisms involved in developing drag load and pile settlement during and post shaking. Finally, recommendations are made regarding the design of piles in liquefiable soils.

2 CENTRIFUGE MODEL TESTS

Two large centrifuge model tests: SKS02 (Sinha et al. 2021c) and SKS03 (Sinha et al. 2021d) were performed on the 9-m radius centrifuge at the Center for Geotechnical Modeling at the University of California Davis. The tests were performed at the centrifugal acceleration of 40g. The numerical quantities presented in this paper have been converted into prototype units per the scaling laws described by Garnier et al. (2007).

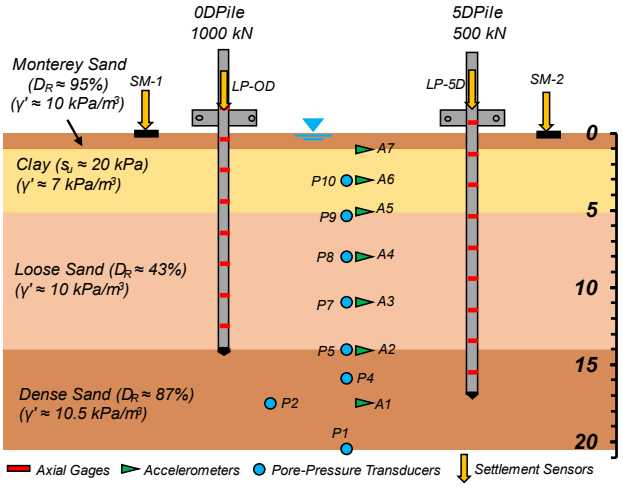

Figure 2. Model cross-section and instrumentation layout for centrifuge test SKS02.

The SKS02 model (Sinha et al. 2021c) consisted of a uniformly layered soil profile of 9 m thick loose liquefiable sand layer (with relative density, $D_R \approx 43\%$) sandwiched between a 4 m layer of relatively low permeable over-consolidated clay (with an undrained shear strength of $s_u \approx 20$kPa) at the top and a dense sand layer ($D_R \approx 87\%$) at the bottom (Figure 2). The clay layer was placed as a slurry and slowly consolidated in stages with pre-consolidation stress of 100 kPa, producing an over-consolidation ratio (OCR) ratio of about 10 at the top and about 4 in the middle of the clay layer. The sand layers consisted of Ottawa F-65 sand with a critical friction angle of 30° (Bastidas 2016). The model consisted of two piles, 0DPile, and 5DPile, loaded with 1000 kN and 500 kN, respectively.

The SKS03 model (Sinha et al. 2021d) had an interbedded soil deposit. The soil profile consisted of 1 m of Monterey sand, 2 m of clay crust ($s_u \approx$ 28-35 kPa), 4.7 m of loose liquefiable sand layer ($D_R \approx 40\%$), 1.3 m of clayey silt layer (20% clay and 80% silt), 4 m of medium dense sand layer ($D_R \approx 60\%$) and a dense sand layer ($D_R \approx 83\%$) beneath it (Figure 3). The clay crust was prepared from a lightly cemented Yolo loam slurry with a water content of w = 50%, soil cement ratio of 3%, and cured for about 2 weeks underwater before the test. The model consisted of two piles (3DPileM and 3DPileL), loaded with 1500 kN and 2400 kN, respectively.

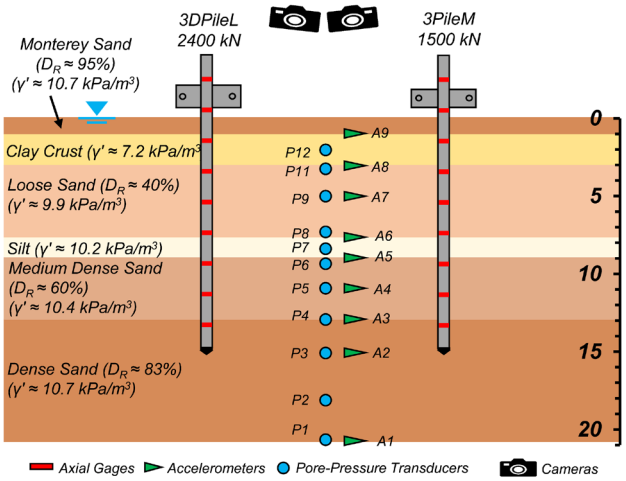

Figure 3. Model cross-section and instrumentation layout for centrifuge test SKS03.

The models consisted of identical pipe piles with an outer diameter (D) of 635 mm and a thickness of 35 mm. The interface of the piles was made significantly rough to achieve the full interface friction angle (Sinha et al. 2021e). The 0D, 3D, and 5D naming annotations in the piles indicate the embedment depth of the pile tip, i.e., the 0DPile had its tip placed at the bottom of the loose sand layer, while the 3D and 5D piles had their tips embedded 3 and 5 times their diameter into the dense sand. The piles were pushed in at 1 g (after placing the soil layers) to their embedment depth by using a crane to lower a heavy mass onto the top of the pile. The static pile capacity for the 0DPile, 3DPiles, and 5DPile were estimated to be 2700 kN, 4000 kN, and 6200 kN, respectively (Sinha et al. 2021c; d). The shaft capacity was calculated by integrating the interface shear strength along the length of the piles (also known as load curve defined later). The tip capacity was taken as the median of the capacity estimated from measured cone penetration at the pile's tip using the empirical methods provided in AASHTO (2020), Lehane et al. (2005), Salgado and Lee (1998), and Titi and Abu-Farsakh 1999). A pile load test was also conducted on 3DPiles in flight, which resulted in a static pile load capacity (estimated from De Beer's 1967 yield load method) of 3800 kN and 4500 kN, respectively at the beginning and at the end of the centrifuge test. The 0DPile and 5DPile loaded with 1000 kN and 500 kN resulted in a static factor of safety of 2.7 and 12.4, respectively (Figure 2). 3DPileM and 3DPileL loaded with 1500 kN and 2400 kN resulted in a static factor of safety of about 2.7 and 1.7, respectively, with the annotations M and L corresponding to the medium and large dead loads applied to produce the safety factors listed (Figure 3).

The models were densely instrumented with accelerometers (A#), pore-pressure transducers (P#), settlement sensors (SM-1, SM-2, LP-0D, LP-5D), and cameras to monitor the generation and dissipation of excess pore pressures, accelerations, and settlement in soil and piles (Figure 2 and Figure 3). The SKS02 model used linear potentiometers LP-0D and LP-5D placed at the center of the pile masses of 0DPile and 5DPile to measure their settlements. Soil settlement was measured by placing the linear potentiometers at the center of soil settlement markers (SM_1 and SM_2). In addition, line lasers and cameras were also used to

measure the settlement of the soil and the piles (Sinha et al. 2021b). The SKS03 model used cameras and digital image correlation (DIC) techniques to obtain 3-D movements of soil and piles (Sinha et al. 2021a). The piles were instrumented with nine strain gages in a full-bridge configuration inside the pile to measure the axial load distribution. The loads applied on the piles were placed closer to the ground (about 1 meter) to avoid the development of large bending moments affecting the axial load measurements in piles. The models were shaken with multiple Santa Cruz earthquake motions while waiting for the complete dissipation of excess pore pressures between each subsequent event. This paper presents the results of a single shaking event, EQM_5 in the SKS02 centrifuge test and EQM_4 in the SKS03 centrifuge test.

3 RESULTS

Shaking events EQM_5 and EQM_4 were the fifth and the fourth events in sequence, respectively, for the centrifuge tests SKS02 and SKS03, respectively. EQM_5 was a scaled Santa Cruz (Northridge 1994 Earthquake) motion with a peak ground acceleration (PGA) of 0.3 g. EQM_4 was a long-duration modified Santa Cruz motion from Malvick et al. (2002) consisting of one large pulse followed by five small pulses, scaled to produce a peak ground acceleration of 0.4g. Figure 4 shows the applied earthquake motion EQM_4 and EQM_5.

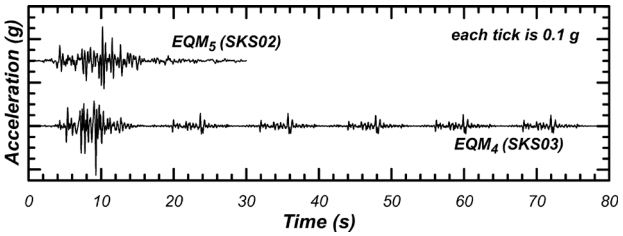

Figure 4. Applied earthquake motion EQM_5 and EQM_4 in centrifuge test SKS02 and SKS03, respectively.

All the piles had developed an initial drag from soil reconsolidation during centrifuge spin up and from following past shaking events. As the centrifuge spun up, gravity progressively increased shear stresses in the soil, which resulted in the development of excess pore pressures, the dissipation of which caused soil reconsolidation resulting in the development of drag load (Sinha et al. 2021e). Before the shaking events of EQM_4 and EQM_5, shakings were of small to medium earthquake motions with peak ground acceleration (PGA) ranging from 0.1 to 0.3 g. The developed drag load on the piles further increased from these previous medium shaking events because of soil reconsolidation following liquefaction. Figure 9 (shown later) shows the initial axial load distribution of the piles at the beginning of shaking events EQM_5 (in centrifuge test SKS02) and EQM_4 (in centrifuge test SKS03). As expected, the axial load distribution in the piles (above the neutral plane) has a parabolic shape showing a linear increase of mobilized interface shear strength with depth. Cone penetration tests conducted between the past shaking events showed relatively uniform soil settlement in the loose sand layer (Sinha et al. 2021c; d). The relatively large increase of axial load in 5DPile at the interface of loose and dense sand could have resulted from the dilatancy of the shear zone around the pile.

Figure 5 and Figure 6 show the distribution of excess pore pressures and settlement in soil and pile, respectively, for shaking events EQM_5 and EQM_4. Figure 7 shows the mobilized tip stress and pile settlement as the free-field effective stress in the soil near the tip changed during and post-shaking. Figure 8 shows the development of liquefaction-induced drag load on 5DPile for shaking event EQM_5. With aid from these figures, the mechanism observed during and post shaking is discussed below.

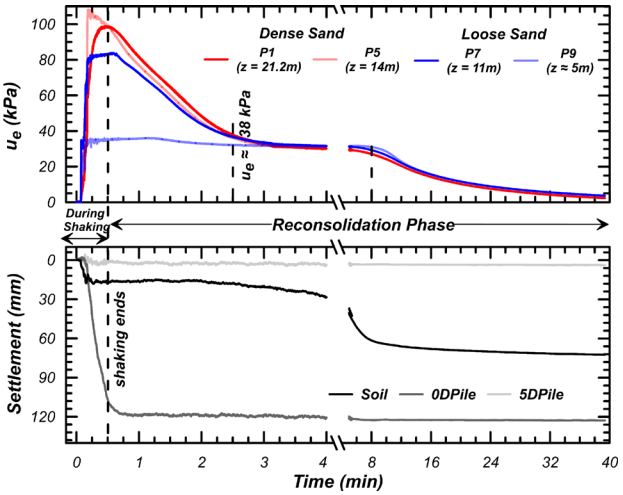

Figure 5. Excess pore pressure distribution and settlement time history for shaking event EQM_5 in centrifuge test SKS02.

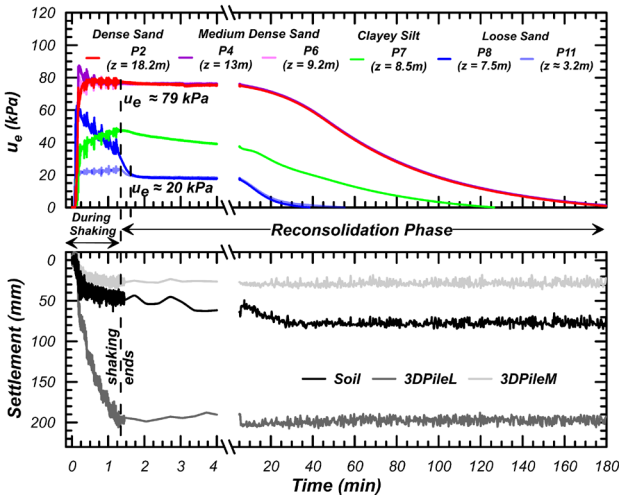

Figure 6. Excess pore pressure distribution and settlement time history for shaking event EQM4 in centrifuge test SKS03

.

3.1 *During Shaking*

Excess pore pressures generated during shaking decreased drag loads; however, it also caused significant settlement in piles. When shaking began, the increase in excess pore pressures (Figure 5 and Figure 6) in soil resulted in the loss of shaft friction and drag load in piles (Figure 8). In Figure 8, the axial loads in the 5DPile decreased as excess pore effective stress decreased during shaking (t = 0s – t = 30 sec). During this period, the drag load in 5DPile decreased from about 700 kN to 300 kN. A decrease in drag load generally decreased the load at the pile's tip. However, since the tip capacity also reduced during shaking, the piles settled until they mobilized enough resistance to attain equilibrium. Figure 7 shows the mobilized tip load and settlement of the pile during shaking.

When full liquefaction was achieved, drag loads significantly reduced; however, the piles suffered significant settlement. When the loose sand layer liquefied, the shaft skin friction in the layer essentially became negligible. In the SKS02 model, the loose sand layered between the depth of 5-12 m was fully liquefied. In the SKS03 centrifuge test, the loose sand and the silt layer were fully liquefied. Figure 8 shows a constant axial load distribution in 5DPile in the liquefied soil (5-12 m), indicating zero drag loads. The decrease in the drag load also decreased the mobilized

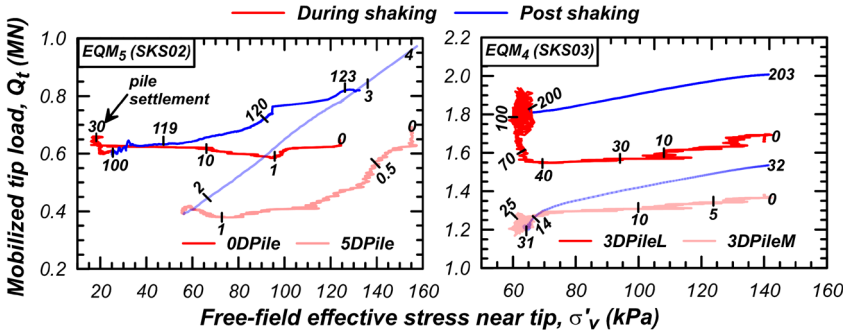

Figure 7. Mobilized tip load (Q_{tip}) and settlement of pile as free-field effective stress at pile's tip depth changed during and post shaking of events: EQM_5 and EQM_4 in centrifuge test SKS02 and SKS03, respectively.

tip load (see 5DPile and 3DPileM in Figure 7). However, for heavily loaded piles, 0DPile and 3DPileL, the loss of shaft friction resulted in more load transferred to its tip, resulting in higher mobilization of tip load than before shaking (see Figure 7). With high excess pore pressures and more load transferred at its tip, the 0DPile and 3DPileL suffered large settlements. At the peak of shaking (when the excess pore pressures were greatest at the pile's tip depth), the 0DPile and the 3DPileL settled by about 80 mm and140 mm, respectively, i.e., about 65% and 70% of their total settlement during the event (Figure 7). Throughout the shaking, the 0DPile and 5DPile settled by 100 mm and <5 mm, respectively, whereas the 3DPileL and 3DPileM suffered 200 mm and 30 mm settlements, respectively. Overall, more than 80-90% of the total pile settlement occurred during shaking. The soil surface also settled during shaking. In SKS02 and SK03 tests, the soil surface settled by 15 mm and 50 mm, respectively.

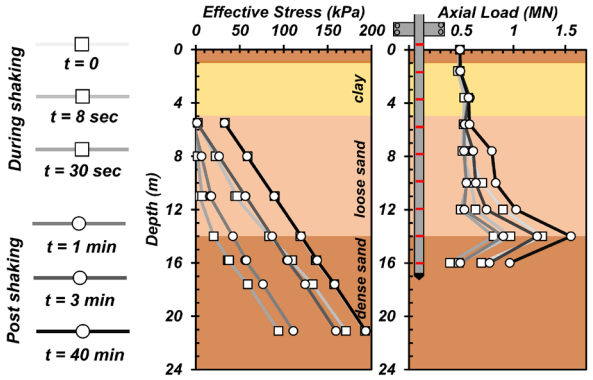

Figure 8. Development of liquefaction-induced downdrag on 5DPile for shaking event EQM_5 in centrifuge test SKS02.

3.2 *During Reconsolidation*

Post shaking, interbedded low permeable layers hindered the drainage of water coming to the surface, causing equalization of excess pore pressures in the layers beneath. When shaking ended (t ≈ 30s for EQM_5 motion and t ≈ 70s for EQM_4 motion), reconsolidation began. The excess pore pressures started to dissipate, and the soil settled. However, the low permeable clay layer and the clayey silt layer slowed down the dissipation rate. It resulted in equalizing excess-pore pressures within all the layers beneath (Figure 5 and Figure 6). In the SKS02 centrifuge test, equalization of excess pore pressures was achieved at t ≈ 2.5 minutes (Figure 5). The excess pore-pressure (u_e) in the layers below the clay layer quickly dissipated and equalized to about u_e ≈ 38 kPa (i.e., the effective stress at the bottom of the clay layer). The impediment of drainage by the clay layer resulted in forming a water film layer at the sand-clay interface (Malvick et al. 2002). During this period, the surface settlement remained almost constant with slight heaving. The water film eventually drained through the leakages from the sides of the centrifuge model container. At t ≈ 8 minutes, the water film entirely disappeared, resulting in about 65 mm of surface settlement. Following that, the excess pore pressure in the soil layers dissipated while remaining equalized, achieving complete reconsolidation in about 45-60 minutes. Similarly, for the SKS03 test, the clay layer and interbedded clayey silt layer resulted in equalization of excess pore-pressures u_e ≈ 20 kPa within the loose sand layer and u_e ≈ 79 kPa within the medium dense and dense sand layers beneath it (Figure 6). In the loose sand layer, complete reconsolidation was achieved in 40 minutes. However, the layers beneath took 3 hours for complete reconsolidation due to the low permeable clayey silt layer. At the end of complete reconsolidation, the soil settled by 73 mm and 78 mm, respectively, in SKS02 and SKS03 tests.

As soil reconsolidated and settled, drag loads increased; however, the settlements of the piles were small. As the excess pore-pressures dissipated, interface shear strength and negative skin friction increased (Figure 8), causing increased drag loads. Consequently, more load was transferred to the tip resulting in an increase of mobilized load at the tip (Figure 7). Figure 8 shows an increase in the axial load distribution in 5DPile as soil reconsolidated. Figure 7 shows an increase in the mobilized tip load during the reconsolidation phase. While the load at the tip increased, the piles were able to resist it by undergoing small settlements. At the end of reconsolidation, the 0DPile settled by about 20 mm, whereas 5DPile, 3DPileL, and 3DPileM settled by less than 10 mm (Figure 5, Figure 6, and Figure 7). Since the 0DPile had its tip at the bottom of the liquefiable layer, some of the pile settlement during reconsolidation could have resulted from the soil settlement beneath it.

3.3 *Discussion on Drag Load*

After complete reconsolidation, the developed drag load (Figure 8) and mobilized tip load (Figure 7) were higher than their initial values before shaking. The increase in the drag load could have resulted from the increase in the lateral earth pressure coefficient (K) from each shaking event. Ganainy et al. (2014) and Kokkali et al. (2018) used tactile pressure sensors in centrifuge model tests and found that the lateral stresses increased post shaking following reconsolidation of liquefied soil. Figure 9 shows the axial load distribution in piles before and after the shaking events. The developed drag load increased with shakings. In the SKS02 test, the magnitude of the drag load was higher (about 1000 kN) for the deeply embedded 5DPile compared to the heavily loaded with shallow embedment 0DPile (460 kN). Correspondingly, the neutral plane in the 5DPile was much deeper, about 14 m, compared to about 11 m for the 0DPile. In the SKS03 test, where piles had the same embedment, the drag loads were higher, and correspondingly the neutral plane was deeper for the lightly loaded 3DPileM. The drag load in 3DPileM was 640 kN compared to the 275 kN in the 3DPileL. The neutral

plane depth was about 9 m for the lightly loaded 3DPileM compared to 5.5 m for the heavily loaded 3DPileL.

A load curve describing the pile capacity was obtained for both the centrifuge tests (Figure 9). A load curve is the integration of the shaft resistance of the pile with depth. The load curve for the SKS03 test was obtained from the pile load test conducted in flight after the end of all shaking events. A load test with a constant penetration rate was conducted to evaluate the pile's interface shear and tip capacity (Sinha et al. 2020c). Figure 9 (a) shows the obtained load curve for 3DPiles. Analysis of the load curve showed mobilization of large lateral stresses around the pile. The lateral stress coefficient (K) around the pile calculated for an interface friction angle of $\delta = 30^o$ was found to increase with depth. The lateral stress coefficient increased from $K \approx 1.4$ at a depth of 4 m to $K = 1.9$ at a depth of 15 m. While the free-field lateral stress coefficient is expected to be around $K = 0.5$ for soil friction angle of $\phi' = 30^o$, a high lateral stress coefficient could develop locally at the pile's interface from arching of soil or dilatancy of the shear zone surrounding the pile. Movement of the pile from the developed drag load during reconsolidation might have resulted in soil arching and dilatancy of the shear zone around the pile resulting in large lateral stress development around the pile. Since no pile load test was conducted for the SKS02 test, the interface shear strength of the pile was estimated as $\tau = K\sigma'_v \tan\delta$ with an interface friction angle of $\delta = 30^o$ and lateral stress coefficient with an average $K = 1$. For the shaft friction in the clay layer, α method of AASHTO (2020) with an undrained shear strength $s_u \approx 20$ kPa was used. Figure 9 (b) shows the calculated load curve for piles in the SKS02 centrifuge test. The figure shows that the final axial load distribution after complete reconsolidation is well contained within the load curve. The loads at the neutral plane are close to the one estimated from the load curve. While some portions of the pile length achieved negative skin friction equal to the assumed interface shear strength, others were not. Overall, the results suggest that liquefaction-induced downdrag can mobilize negative skin friction up to 100% of the interface shear strength in the liquefied as well as non-liquified soils. However, the true magnitude and distribution of the negative skin friction developed at the interface will depend on the soil-pile interaction during the shaking event.

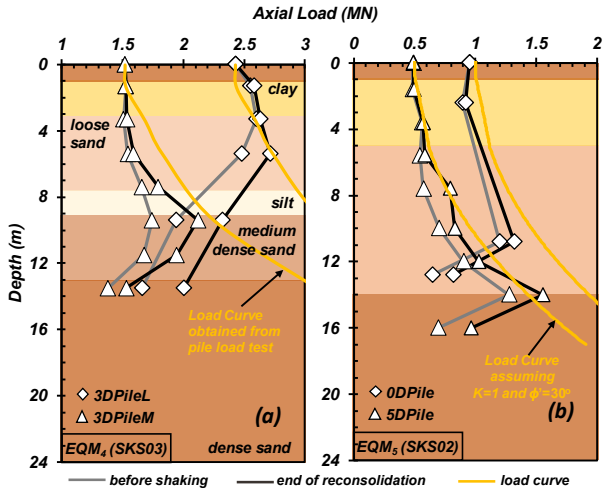

Figure 9. Distribution of axial load in piles before and after the shaking event (a) EQM_4 in centrifuge test SKS04 and (b) EQM_5 in centrifuge test SKS02.

A small settlement in the soil can cause a significant increase in drag loads. In the SKS03 centrifuge test, about 20-25 mm of soil settlement (during reconsolidation) achieved full drag load on piles (Figure 6). Soil settlement of 20-25 mm equals about 3-4% of the pile diameter. Fleming et al. (2008) suggested that shear displacements of 0.5% to 3% of the pile diameter are required to mobilize full shaft resistance. Viewed another way, the 20 mm of soil settlement corresponds to a displacement equal to 2.5 times the median grain diameter (D_{50}) of sand used in the centrifuge test. DeJong and Westgate (2009) and Martinez and Frost (2017) suggested an interface shear band thickness of 5–7 particle diameters adjacent to the pile's interface. A relative movement of soil by 3 x D_{50} (assuming a shear band thickness of 5 x D50) would produce a shear strain of 50%, which would likely be enough to mobilize the full negative skin friction at the interface. These results suggest that even when the soil layers do not fully liquefy, settlements caused by the dissipation of excess pore pressures exceeding a small percentage of the pile diameter would be enough to mobilize large negative skin friction at the interface.

4 CONCLUSIONS

Two large centrifuge model tests were conducted to study liquefaction-induced downdrag on piles. The model consisted of four heavily instrumented medium pipe piles with an outer diameter of 635 mm with a thickness of 35 mm with their tip embedded zero, three, and five times their diameter in the dense sand. Nine strain gages were installed inside the inner diameter to measure the axial load distribution along the length of the piles. The piles were made rough to achieve maximum interface shear strength. The models consisted of two different soil profiles with liquefiable layers and interbedded deposits. The model was shaken with strong earthquake motions, and the developed downdrag was monitored. Results on the mechanism of liquefaction-induced downdrag, drag load, and soil and pile settlement were presented. The main findings from the experiment, which should be accounted for designing piles in liquefiable soils, are described below.

- During shaking, excess pore pressure in the soil resulted in the loss of shaft friction and decreased drag load. When the soil was fully liquefied ($r_u \approx 1$), the drag load in the liquefied layer essentially became zero. Post shaking, as soil reconsolidated, drag load gradually increased, surpassing the initial value before shaking. The increase in drag load can be attributed to the increase in lateral stress coefficient (K) from densification caused by the shaking events. The developed drag load was higher for the piles which were lightly loaded or embedded deep in the soil.
- Soil settlements in the order of 1% of the pile's diameter or a couple of particle diameters are sufficient to mobilize significant negative skin friction at the interface. Furthermore, the results show that negative skin friction in the liquefied and the non-liquefied layer can reach up to 100% of the drained interface shear strength. The load curve estimated from the full mobilization of interface shear strength enveloped the axial load distributions in piles.
- Most of the pile settlements occurred during shaking when the excess pore pressures were high. With reduced tip capacity and more load transferred to the tip, the pile underwent settlement until enough tip resistance was mobilized to achieve equilibrium. Overall, 80-90% of the pile settlements occurred during shaking. For design, it is recommended to check the settlement of the piles during shaking by considering the reduced shaft and tip capacities from the presence of excess pore pressures in the soil. Post-shaking, the observed settlements in piles were generally small (< 10 mm).

Liquefaction-induced downdrag did not result in strength failure (from the developed drag load) or serviceability failure (i.e., significant settlement of pile). While large drag loads developed, the piles were able to sustain them by undergoing small

settlements. A settlement-based approach is therefore recommended to design piles for downdrag. Test results showed that the piles of sufficient structural strength and capacity satisfying the serviceability criterion during shaking are overall safe and undergo small settlements during reconsolidation.

5 ACKNOWLEDGEMENTS

This work was funded by the California Department of Transportation under Agreement 65A0688 and National Science Foundation award number CMMI 1635307. The authors would like to acknowledge Caltrans engineers and staff involved in this project for their suggestions and assistance. The support provided by the UC Davis Center for Geotechnical Modeling and staff during the conduct of the centrifuge tests is greatly appreciated. The paper was significantly improved, subjected to the comments and suggestions of the two anonymous reviewers. Their insights are appreciated.

6 REFERENCES

AASHTO (2020). *AASHTO LRFD Bridge design specifications*. LRFDUS-9, Washington, DC.

Bastidas A.M.P. (2016). *Ottawa F-65 Sand Characterization*. Ph.D. Dissertation, University of California Davis.

Boulanger R.W. and Brandenberg S.J. (2004). Neutral plane solution for liquefaction-induced down-drag on vertical piles. *GeoTrans*, 470–478.

Caltrans (2020). Liquefaction-induced downdrag. *Caltrans Geotechnical Manual.*

DeJong J.T. and Westgate Z.J. (2009). Role of initial state, material properties, and confinement condition on local and global soil-structure interface behavior. *J. Geotech. Geoenviron. Eng.,* 135(11), 1646–1660.

Fellenius B.H. (1984). Negative skin friction and settlement of piles. *Proc. 2nd Int. Seminar - Pile Foundations*, Nanyang Technological Institute, Singapore, 12–24.

Fellenius B.H. (2004). Unified design of piled foundations with emphasis on settlement analysis. *Current Practices and Future Trends in Deep Foundations*, Los Angeles, California, 253–275.

Fellenius B.H. and Siegel T.C. (2008). Pile drag load and downdrag in a liquefaction event. *J. Geotech. Geoenviron. Eng.*, 134(9), 1412–1416.

Fleming K., Weltman A., Randolph M., and Elson K. (2008). *Piling Engineering*, John Wiley & Sons, London.

Ganainy, H. El, Tessari, A., Abdoun, T., and Sasanakul, I. (2014). Tactile pressure sensors in centrifuge testing. *Geotech. Test. J.*, 37(1), 151-163. https://doi.org/10.1520/GTJ20120061.

Garnier J., Gaudin C., Springman S.M., Culligan P.J., Goodings D., Konig D., Kutter B., Phillips R., Randolph M.F., and Thorel L. (2007). Catalogue of scaling laws and similitude questions in geotechnical centrifuge modelling. *Int. J. Phys. Model. Geotech,* 7(3), 01–23.

Hannigan P.J., Rausche F., Likins G.E., Robinson B.R., and Becker M.L. (2016). *Design and Construction of Driven Pile Foundations*. FHWA-NHI-16-009, Federal Highway Administration, Woodbury, Minnesota.

Kokkali, P., Abdoun, T., and Zeghal, M. (2018). Physical modeling of soil liquefaction: Overview of LEAP production test 1 at Rensselaer Polytechnic Institute. *Soil Dyn. and Earthq. Eng.*, 113, 629–649.

Lehane, B. M., Schneider, J. A., and Xu, X. (2005). *A Review of Design Methods for Offshore Driven Piles in Siliceous Sand*. GEO:05358, University of Western Australia.

Malvick E.J., Kulasingam R., Boulanger R.W., and Kutter B.L. (2002). *Effects of void redistribution on liquefaction flow of layered soil – centrifuge data report for EJM01*. UCD/CGMDR-02/02, Center for Geotechnical Modeling, University of California Davis.

Martinez A. and Frost J.D. (2017). The influence of surface roughness form on the strength of sand–structure interfaces. *Géotechnique Letters*, 7(1), 104–111.

Rollins K.M. and Strand S.R. (2006). Downdrag forces due to liquefaction surrounding a pile. *Proc. 8th National Conf. Earthq. Eng.,* San Francisco, California.

Rollins K.M. and Strand S.R. (2007). *Liquefaction Mitigation Using Vertical Composite Drains: Full-Scale Testing for Pile Applications*. Transportaion Research Board, Provo, Utah.

Salgado, R., and Lee, J. (1998). *Pile Design Based on Cone Penetration Tests*. FHWA/IN/JTRP-99/8, Joint Transportation Research Program, Indiana Department of Transportation.

Sinha, S. K., Kutter, B. L., Wilson, D. W., Carey, T., and Ziotopoulou, K. (2021a). *Use of Photron cameras and TEMA software to measure 3D displacements in centrifuge tests*. UCD/CGM - 21/01, Center for Geotechnical Modeling, University of California Davis.

Sinha, S. K., Kutter, B. L., and Ziotopoulou, K. (2021b). Measuring Vertical Displacement using Laser Lines and Cameras. *Under 2nd Review*.

Sinha, S. K., Ziotopoulou, K., and Kutter, B. L. (2021c). *Centrifuge testing of liquefaction-induced downdrag on axially loaded piles : Data Report for SKS02*. UCD/CGMDR - 21/01, Center for Geotechnical Modeling, University of California Davis.

Sinha, S. K., Ziotopoulou, K., and Kutter, B. L. (2021d). *Centrifuge testing of liquefaction-induced downdrag on axially loaded piles : Data Report for SKS03*. UCD/CGMDR - 21/02, Center for Geotechnical Modeling, University of California Davis.

Sinha, S. K., Ziotopoulou, K., and Kutter, B. L. (2021e). Centrifuge Model Tests of Liquefaction Induced Downdrag on Piles in Uniform Liquefiable Deposits. *Under Review*.

Titi, H., and Abu-Farsakh, M. Y. (1999). *Evaluation of Bearing Capacity of Piles From Cone Penetration Test Data*. LTRC Project No. 98-3GT Louisiana Transportation Research Center.